Journal of Controlled Release 197 (2015) 69–77

Contents lists available at ScienceDirect

Journal of Controlled Release

journal homepage: www.elsevier.com/locate/jconrel

Mathematical model accurately predicts protein release from an affinity-based delivery system

Katarina Vulic [a,d,1], Malgosia M. Pakulska [b,c,d,1], Rohit Sonthalia [b], Arun Ramachandran [b,*], Molly S. Shoichet [a,b,c,d,**]

[a] Department of Chemistry, University of Toronto, Toronto, Ontario M5S 3E1, Canada
[b] Department of Chemical Engineering and Applied Chemistry, University of Toronto, Toronto, Ontario M5S 3E1, Canada
[c] Institute of Biomaterials and Biomedical Engineering, University of Toronto, Toronto, Ontario M5S 3E1, Canada
[d] The Donnelly Centre for Cellular and Biomolecular Research, University of Toronto, Toronto, Ontario M5S 3E1, Canada

ARTICLE INFO

Article history:
Received 24 October 2014
Accepted 31 October 2014
Available online 6 November 2014

Keywords:
Affinity release
Controlled release
Protein release
Mathematical modeling
Dimensionless analysis
Protein stability

ABSTRACT

Affinity-based controlled release modulates the delivery of protein or small molecule therapeutics through transient dissociation/association. To understand which parameters can be used to tune release, we used a mathematical model based on simple binding kinetics. A comprehensive asymptotic analysis revealed three characteristic regimes for therapeutic release from affinity-based systems. These regimes can be controlled by diffusion or unbinding kinetics, and can exhibit release over either a single stage or two stages. This analysis fundamentally changes the way we think of controlling release from affinity-based systems and thereby explains some of the discrepancies in the literature on which parameters influence affinity-based release. The rate of protein release from affinity-based systems is determined by the balance of diffusion of the therapeutic agent through the hydrogel and the dissociation kinetics of the affinity pair. Equations for tuning protein release rate by altering the strength (K_D) of the affinity interaction, the concentration of binding ligand in the system, the rate of dissociation (k_{off}) of the complex, and the hydrogel size and geometry, are provided. We validated our model by collapsing the model simulations and the experimental data from a recently described affinity release system, to a single master curve. Importantly, this mathematical analysis can be applied to any single species affinity-based system to determine the parameters required for a desired release profile.

1. Introduction

The advent of controlled release systems is transforming the field of drug delivery, offering improved pharmacokinetics, minimized dosing, and safer treatments. There are several methods to control the rate of therapeutic release, including encapsulation in degradable polymeric particles [1,2] or rods [3,4] and affinity-based systems [5,6]. Affinity-based release systems are particularly interesting because they do not require organic solvents and high shear stress for fabrication, which can degrade some therapeutics. This is especially important for the increasing number of protein therapeutics being investigated [7]. Although previously often limited to heparin-binding proteins [8–15], new, broadly applicable affinity release systems are now emerging [5,16]. Despite this exciting new approach to control release, a comprehensive understanding of how release of therapeutic agents from such systems can be modulated is often limited to trial-and-error experimentation, rendering the process resource and time intensive. A mathematical model is warranted to provide insight into which factors are most important to control the rate of therapeutic release from affinity-based delivery systems, and how these factors can be modulated to obtain a desired release profile.

Several groups have previously used mathematical models to predict release profiles of small molecules or proteins from various affinity-based hydrogels. Sakiyama-Elbert and coworkers have extensively investigated and modeled the release of heparin-binding growth factors from heparin-binding peptides immobilized within a fibrin scaffold. This complex system uses two independent affinity interactions to govern protein release: that of heparin with the immobilized heparin-binding peptides and that of the growth factors with heparin [8,9,17,18]. Lin and Metters used a mathematical model to understand the *in vitro* release of hexahistidine tagged green fluorescent protein or bovine serum albumin from metal-chelating hydrogels [19,20]. Similarly, Fu et al. modeled

* Corresponding author.
** Correspondence to: M.S. Shoichet, Department of Chemistry, University of Toronto, Toronto, Ontario M5S 3E1, Canada.
E-mail addresses: arun.ramachandran@utoronto.ca (A. Ramachandran), molly.shoichet@utoronto.ca (M.S. Shoichet).
[1] These authors contributed equally to this work.

http://dx.doi.org/10.1016/j.jconrel.2014.10.032
0168-3659/

release of hydrophobic small molecules from cyclodextrin hydrogels [21]. More recently, Koehler and coworkers modeled the release of a low molecular weight peptide from a polyethylene glycol hydrogel [22], while Fan et al. modeled release of PDGF-BB from aptamer-functionalized hydrogels [23]. These models have broadened our understanding of the mechanisms controlling affinity-based protein release from hydrogels; however, no general guiding equations in terms of the kinetic constants, gel thickness, protein diffusivity, and binding ligand concentration, among other factors, have emerged from these studies. Furthermore, there have been inconsistencies in the observations of factors affecting release. For example, some groups have noticed that the dissociation kinetics of the complex impact release [19] whereas others have found these kinetics to be irrelevant (personal communication, [17]). The type of release profile observed has varied between different affinity systems and within the same system. Some groups observed a single timescale of release [17], others two timescales of release [24], and others a combination of the two [25]. Finally, the effect of hydrogel geometry has yet to be investigated.

In this work, we used a mathematical model to simulate affinity-based protein release from a model affinity-based system comprised of an injectable hydrogel scaffold modified with SH3-binding peptides and a therapeutic fusion protein, such as recombinant human fibroblast growth factor 2, expressed with the Src homology 3 domain (SH3-rhFGF2) (Fig. 1) [5]. This system is broadly applicable to any protein that can be expressed as a fusion with SH3 and has been recently demonstrated with another protein, chondroitinase ABC [16]. This model, describing a single species affinity system, was first shown by Lin and Metters [19] and subsequently used by others [21–23]. We demonstrate agreement between the model and these experimental systems and we also delineate simple inequalities that demonstrate how binding affinity (K_D), the concentration of binding ligand, rate of dissociation (k_{off}), and hydrogel thickness and geometry affect the protein release profile. Interestingly, protein concentration does not affect release dynamics (see Supplementary Information Fig. S1). Importantly, this model provides new insight into the capabilities and limitations of single species affinity-based delivery systems, and also provides design guidelines to achieve desired release profiles.

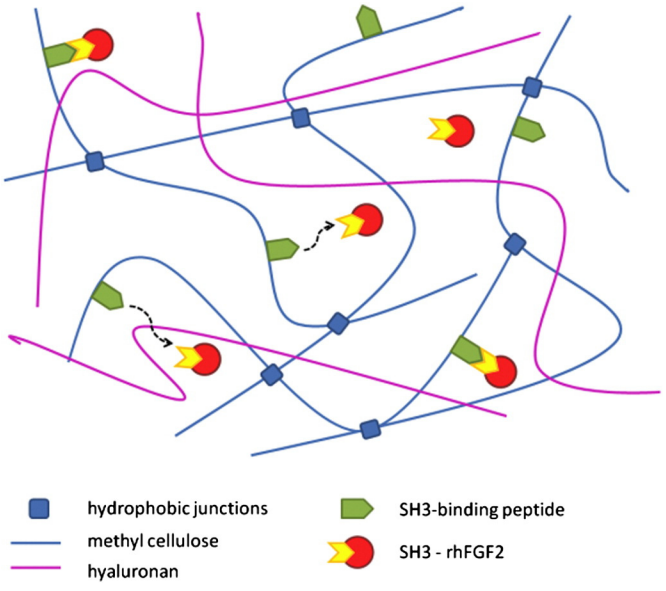

Fig. 1. Affinity between hydrogel-bound SH3-binding peptides and the SH3 domain controls the release of a therapeutic fusion protein, SH3-rhFGF2. Reprinted with permission from [5]. Copyright 2011 American Chemical Society.

2. Materials and methods

2.1. Mass transport dynamics

Simple binding kinetics, similar to those previously described by Crank [26], were used to model affinity-based controlled release. The experimental systems that we modeled were those of SH3-rhFGF2 and SH3-ChABC from hydrogels modified with SH3-binding peptides. Importantly, the model parameters used herein were not obtained through regression analysis, but rather independently measured or chosen to reflect our specific system. The model parameters used in the generation of each figure are detailed in Table S2. The experimental data validates the adequacy of the model to describe this type of system. Thus, any physically valid parameters can be used to predict the release of a protein from an affinity-based controlled release system.

Several assumptions relevant to the model are detailed in the supplementary information (SI). The affinity-based system controls release of freely diffusible SH3-rhFGF2 or SH3-ChABC (protein) through an equilibrium reaction between the protein and immobilized SH3-binding peptide (peptide), which forms an immobilized protein–peptide complex (complex). Fig. 2A shows a schematic diagram of the experimental release system including the transport processes occurring in each region. The hydrogel serves as a scaffold material in the system. The conical geometry used in the mathematical model mimics that of the experimental *in vitro* release system and can be changed for other geometries. The rates of association (k_{on}) and dissociation (k_{off}), commonly expressed as the dissociation constant (K_D), determine the strength of the affinity interaction (Eq. (1)), which regulates protein release from the hydrogel into the release media.

$$K_D = \frac{k_{off}}{k_{on}} = \frac{C_{pro} \cdot C_{pep}}{C_{com}} \tag{1}$$

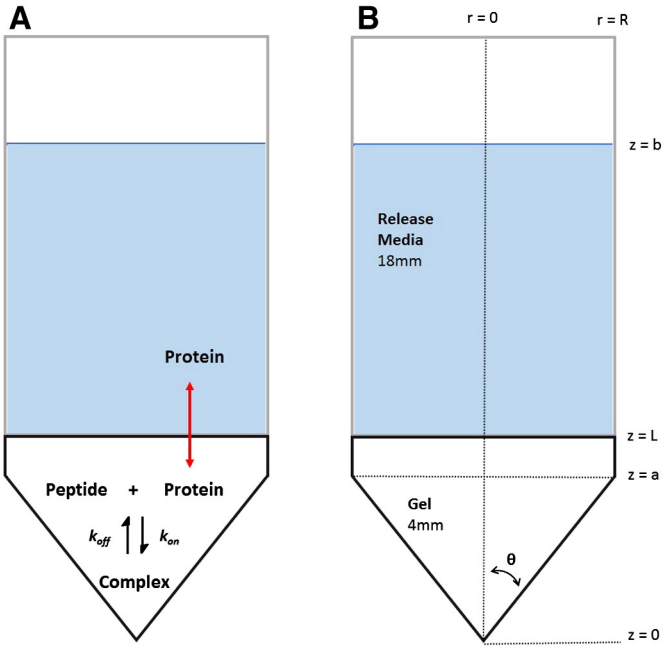

Fig. 2. Schematic diagram for affinity-based delivery from hydrogels modified with SH3-binding peptides. The conical geometry is incorporated in the model to mimic the *in vitro* experimental methodology. A) Transport processes within the system. Freely diffusible SH3-rhFGF2 or SH3-ChABC (protein) can reversibly bind to hydrogel-immobilized SH3-binding peptides (peptide) to form an immobilized peptide–protein complex (complex). B) The geometry of the system. The hydrogel spans $z = 0$ to $z = L$(4 mm height) and the release media spans $z = L$ to $z = b$ (18 mm for SH3-rhFGF2 and 7.6 mm for SH3-ChABC). The conical portion of the tube spans $z = 0$ to $z = a$(3.2 mm). Theta (θ) is the angle of the tube from the vertical (54.6°) and R (4.5 mm) is the radius of the tube.

Here, C_{pro}, C_{pep} and C_{com} are the molar concentrations of the free protein in the gel matrix, the uncomplexed or free peptide and the complexed or bound peptide, respectively. Diffusivity of SH3-rhFGF2 or SH3-ChABC (D_{pro}) through the hydrogel and release media was estimated using a modified Stokes–Einstein–Sutherland equation (Eq. (2)) where: T is the temperature (K); μ is the viscosity of the release media (water is used as an estimate); and MW_{pro} is the molecular weight of the fusion protein SH3-rhFGF2 or SH3-ChABC [27]. It was assumed that protein diffusivity through the gel and release media were not significantly different as the hydrogel is highly water-swollen (96% water w/w) and its pore sizes are significantly greater than the size of the protein [28,29].

$$D_{pro} = \frac{9.940x10^{-15} \cdot T}{\mu \cdot \sqrt[3]{MW_{pro}}} \tag{2}$$

The mass transport within the hydrogel can be described using mass balances for protein and complex. The concentration of free protein (C_{pro}) changes due to diffusion from the gel as well as association or dissociation with the bound peptide:

$$\frac{\partial C_{pro}}{\partial t} = \frac{D}{r}\frac{\partial}{\partial r}\left(r\frac{\partial C_{pro}}{\partial r}\right) + D\frac{\partial^2 C_{pro}}{\partial z^2} - k_{on}C_{pro}\left(C_{pep,T} - C_{com}\right) + k_{off}C_{com}. \tag{3}$$

Due to the nature of the geometry, we have employed the axisymmetric cylindrical co-ordinate system (r, z), where r is the radial distance from the axis, and z is the axial co-ordinate measured from the base of the tube.

The concentration of complex (C_{com}) relies only on the equilibrium binding:

$$\frac{\partial C_{com}}{\partial t} = k_{on}C_{pro}\left(C_{pep,T} - C_{com}\right) - k_{off}C_{com}, \tag{4}$$

where the concentration of free peptide (C_{pep}) is described as a difference between the concentration of total immobilized peptide ($C_{pep,T}$) and the concentration of complex (C_{com}).

$$C_{pep} = C_{pep,T} - C_{com}.$$

Due to the geometry, the boundary conditions in the radial direction must be split into two regions, the conical portion and the cylindrical portion. This geometry was selected to mimic the *in vitro* experimental conditions; however, it may be easily adjusted in COMSOL to reflect more relevant *in vivo* geometries (e.g. disc, plane sheet).

In the conical region:

$$\frac{\partial C_{pro}}{\partial r} = 0 (r = 0),$$

and

$$\hat{n} \cdot \nabla C = 0 \ (r = z tan\theta, z < a),$$

where θ is the tube angle from the vertical and $\hat{n}$ is the unit normal to the conical surface.

In the cylindrical region:

$$\frac{\partial C_{pro}}{\partial r} = 0 (r = 0),$$

and

$$\frac{\partial C_{pro}}{\partial r} = 0 (r = R,\ z > a),$$

where R is the outer radius of the tube.

In the z direction, the boundary conditions reflect no diffusion through the bottom of the tube, equality of flux at the media–gel interface (with equal diffusivities in the gel and media) and no partition coefficient between the gel and the media.

$$\frac{\partial C_{pro}}{\partial z} = 0 \quad (z = 0)$$
$$\frac{\partial C_{pro}}{\partial z}(gel) = \frac{\partial C_{pro}}{\partial z}(media) \quad (z = L)$$
$$C_{pro,gel} = C_{pro,media} \quad (z = L)$$

The initial conditions in the gel reflect equilibrium between free and bound protein:

$$C_{pro}(t = 0) = C_{pro}^{eq},$$

and

$$C_{com}(t = 0) = C_{com}^{eq}.$$

Within the media, the transport of free protein is due only to diffusion:

$$\frac{\partial C_{pro}}{\partial t} = \frac{D}{r}\frac{\partial}{\partial r}\left(r\frac{\partial C_{pro}}{\partial r}\right) + D\frac{\partial C_{pro}^2}{\partial z^2}. \tag{5}$$

In this domain, the geometry is only cylindrical, therefore the boundary conditions in the radial direction are:

$$\frac{\partial C_{pro}}{\partial r} = 0 \quad (r = 0),$$

and

$$\frac{\partial C_{pro}}{\partial r} = 0 \quad (r = R).$$

As before, at the media–gel interface, the boundary conditions in the z direction reflect equal diffusivity and no partition coefficient between the gel and the media

$$\frac{\partial C_{pro}}{\partial z}(gel) = \frac{\partial C_{pro}}{\partial z}(media) \quad (z = L),$$
$$C_{pro,gel} = C_{pro,media} \quad (z = L)$$

and no protein diffusion from the media into the air at the media–air interface:

$$\frac{\partial C_{pro}}{\partial z} = 0 \quad (z = b).$$

In the media, the initial concentration of protein is 0.

$$C_{pro}(t = 0) = 0.$$

The equations were rendered dimensionless and solved in the commercially available software, COMSOL. The cumulative percent of protein released at each time point corresponding to experimental conditions was calculated by integration of protein concentration over the entire release media volume. The procedure is explained in detail in SI and the model parameters used for each simulation are detailed in Table S2.

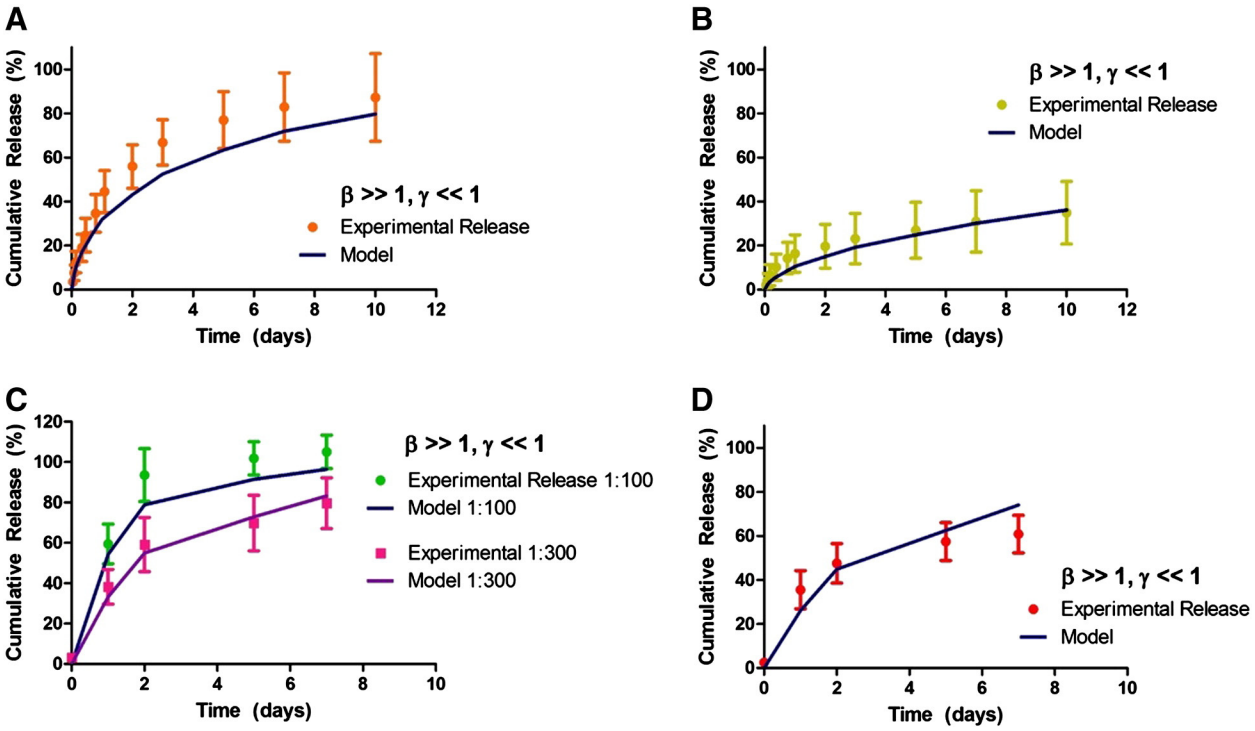

Fig. 3. Model simulation (solid lines) and experimental release data (data points) show good agreement for release of SH3-rhFGF2 from a hydrogel modified with A) weak binding peptide or B) strong binding peptide; and SH3-ChABC from a hydrogel modified with C) weak binding peptide or D) strong binding peptide. The notations 1:100 and 1:300 indicate the ratio of protein to peptide for C). For the SH3-rhFGF2 experimental release data, $n = 4$, mean ± standard deviation plotted; and for SH3-ChABC experimental release data, $n = 3$, mean ± standard deviation plotted. Lines between the data points correspond to the model predictions and are included as a visual guide.

2.2. Experimental release assay

2.2.1. Release of SH3-rhFGF2

The experimental release of SH3-rhFGF2 was previously described [5]. Briefly, 100 μL of peptide-modified hydrogel containing SH3-rhFGF2 (20 μM) was injected into the bottom of a 2.0 mL conical microcentrifuge tube. 900 μL of pre-warmed artificial cerebrospinal fluid (aCSF) with 0.2 mg/mL heparin (release media) was added to each tube and samples were incubated at 37 °C on an orbital shaker. Release media was fully removed and replaced with fresh release media at $t = 1, 2, 4, 8, 16, 24, 48, 72, 120, 168$ and 240 h. Aliquots were frozen at −20 °C until assayed for SH3-rhFGF2. A sandwich ELISA (Peprotech, Human FGF-basic ELISA Development Kit) was used to determine the concentration of SH3-rhFGF2 in the release media removed at each time point ($n = 4$).

2.2.2. Release of SH3-ChABC

The experimental release of SH3-ChABC was previously described [16]. Briefly, 100 μL of peptide-modified hydrogel containing SH3-ChABC (4.56 μM) was injected into the bottom of a 2.0 mL conical microcentrifuge tube. The tubes were pre-warmed at 37 °C for 10 min to allow the gels to set and 400 μL of aCSF was then carefully placed on top of the gel. The gels were kept in a 37 °C incubator with gentle shaking. At designated time points (0, 1, 2, 5, and 7 days) the supernatant was

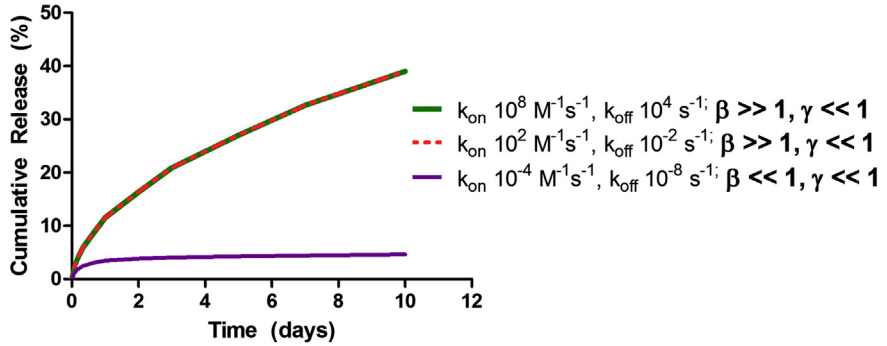

Fig. 4. Model simulations for a K_D of 10^{-4} M with different k_{on} and k_{off} values. For physically relevant rates ($k_{off} > 10^{-2}$ s^{-1}, green and red curves), protein release is unperturbed by varying the binding kinetics. Theoretically, the release would change with very slow unbinding dynamics (k_{off} 10^{-8} s^{-1}, purple curve); however, these rates are not physically relevant for protein–protein interactions. For interpretation of the references to color in this figure legend, the reader is referred to the web version of this article.

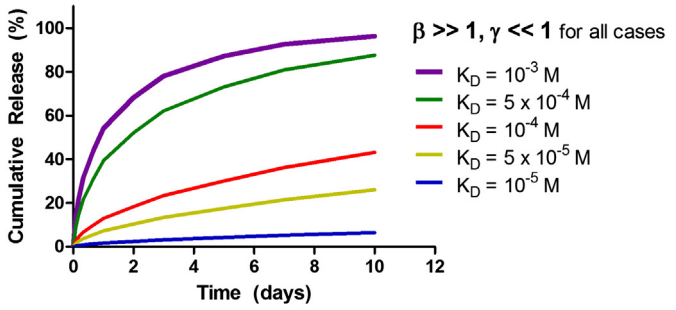

Fig. 5. The model predicts that tunable protein release rates can be achieved by adjusting the strength of the affinity interaction from weak ($K_D = 10^{-3}$ M) to strong ($K_D = 10^{-5}$ M) for a protein to peptide ratio of 1:100. For these simulations, K_D was varied by modulating k_{off}, while k_{on} was held constant at 1×10^8 M^{-1} s^{-1}.

completely removed and replaced with fresh aCSF. Release samples were stored at −80 °C until analysis by ELISA ($n = 3$).

3. Results

3.1. Dimensionless parameters

When our model is rendered dimensionless (see SI, Section S2) [21], three dimensionless parameters emerge in the equations:

$$\alpha = \frac{C_{pro,0}}{C_{pep,\,T}}$$
$$\beta = \frac{L^2 k_{off}}{D}$$
$$\gamma = \frac{k_{on} C_{pro,0}}{k_{off}} = \frac{C_{pro,0}}{K_D}$$

Alpha (α) represents the amount of free protein ($C_{pro,0}$) at the beginning of the experiment relative to the total amount of peptide ($C_{pep,T}$). This term is influenced by the K_D of the protein–peptide pair since the system is assumed to be initially at equilibrium. Note that α is a measure of the *free* protein in the gel. The total concentration of protein in the gel in both free and bound forms initially is $C_{pep,T}\left(\alpha + \frac{\gamma}{\gamma+1}\right)$. Beta ($\beta$) relates the timescale of protein diffusion to the timescale of dissociation of the complex. This term is dependent on the geometry of the hydrogel (L), the dissociation rate of the complex (k_{off}) and the diffusivity of the protein through the gel (D). Gamma (γ) is the concentration of complexed peptide sites in the gel relative to the uncomplexed ones at the beginning of the experiment. Since the initial concentration of the complex is $C_{pep,T}\frac{\gamma}{\gamma+1}$, for $\gamma \gg 1$, most of the peptides are in the complexed state initially. Conversely, if $\gamma \ll 1$, only a small fraction of peptide has bound protein. This term is ultimately governed by K_D ($\frac{k_{off}}{k_{on}}$) and the amount of free protein at the beginning of the experiment.

3.2. Simulation results

We validated our model by comparing model simulations with the experimental data at the experimental time points for the release of both SH3-rhFGF2 and SH3-ChABC from SH3-binding peptide modified hydrogels. The exact values for L, D, C_{pro}, and $C_{pep,T}$ were known from the experimental conditions. The K_D was measured using isothermal titration calorimetry (ITC, SI, Section S4, Table S1) and reasonable k_{on} and k_{off} rates were approximated based on measured rates for another SH3 binding domain [30]. Importantly, none of the model parameters were obtained by fitting. We observed very good agreement between model simulations and experimental data for both proteins (Fig. 3). Diffusional release of SH3-rhFGF2 from an unmodified hydrogel (no peptide) was also well predicted by the model (SI, Fig. S4). The experimental data were corrected for protein loss during sample processing (SI, Figs. S5, S6 and S7). While protein fragility due to aggregation, thermal instability and denaturation is well-known [31,32], it is seldom accounted for in many controlled release systems.

3.3. Effect of association (k_{on}) and dissociation (k_{off}) kinetics on protein release

We investigated how protein release from affinity-based systems is affected by various system parameters, using the SH3 affinity-based system as an example. In the experimental affinity-based system that we used, the k_{on} and k_{off} rates for the Abp1p (actin-binding protein in *Saccharomyces cerevisiae*) SH3 domain are unknown; however, the Fyn SH3 domain (SH3 region of the Fyn protein in *Homo sapiens*) is known to have a k_{on} rate in the range of 10^8 M^{-1} s^{-1} and a k_{off} rate range of 1–10^2 s^{-1} [30]. Since the rate of association tends to be more consistent between binding pairs than the rate of dissociation and there is high conservation of the SH3 domain across species [33], we assumed that the Abp1p domain would have a similar rate of association to that of the Fyn domain. The rate of dissociation then follows from the relationship $K_D = k_{off}/k_{on}$.

We investigated whether protein release from our system could be perturbed by varying k_{on} and k_{off} while keeping $K_D = k_{off} / k_{on}$ constant at the measured order of magnitude (10^{-4} M). Protein release was unperturbed by changes in the individual values of k_{on} and k_{off} (Fig. 4, green and red curves overlap) as long as physically relevant rates of protein association and dissociation were used (k_{on} 10^8–10^2 M^{-1} s^{-1} and k_{off} 10^4–10^{-2} s^{-1}). A change in predicted release profile was only observed when physically irrelevant values were used for k_{on} and k_{off} (10^{-4} M^{-1} s^{-1} and 10^{-8} s^{-1}, respectively; Fig. 4, purple curve) [34,35]. This demonstrates the importance of using physically relevant terms in simulations.

3.4. Effect of K_D on protein release

Model simulations were used to investigate the effect of K_D on protein release for a protein to peptide ratio similar to that used in experimental studies (1:100). Fig. 5 shows that protein release can be tuned

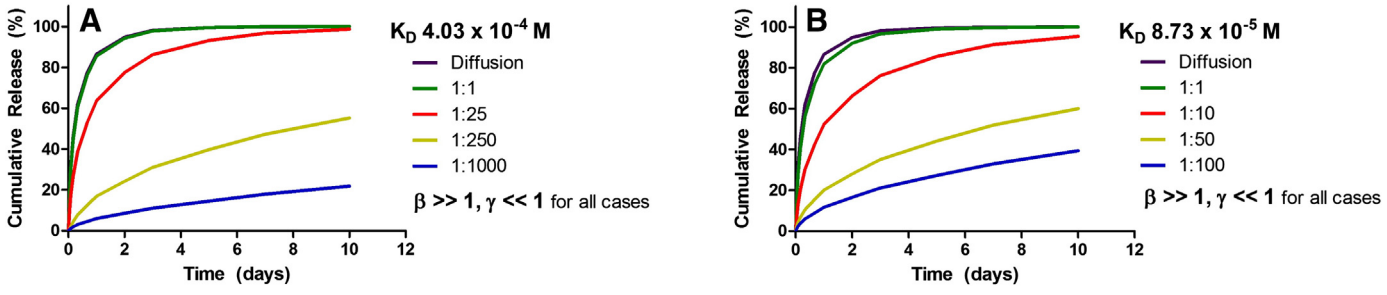

Fig. 6. Tunable protein release from the A) weak binding peptide and B) strong binding peptide affinity systems can be achieved by carefully selecting the initial ratio of protein to peptide.

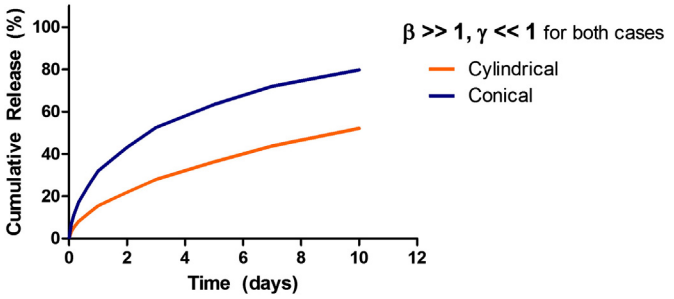

Fig. 7. Model simulation for protein release from hydrogels modified with the weak SH3-binding peptide using a conical versus cylindrical geometry.

by varying the K_D of the protein–peptide interaction (k_{on} was kept constant, and k_{off} was varied). Interestingly, the model predicts that a weak interaction (10^{-3} M) does not appreciably attenuate diffusional release (~80% release by day 3) whereas a strong interaction (10^{-5} M) slows protein release significantly such that only <10% of total protein is released by day 10.

3.5. Effect of protein to peptide ratio on protein release

We used the model to examine the effect of the initial protein to peptide ratio on protein release from affinity hydrogels modified with either strong or weak binding peptides. In these simulations, the peptide concentration was varied while the protein concentration was held constant (Fig. 6). The diffusion curve was estimated using an extremely low concentration of peptide (1000× lower than protein). For the weak binding peptide system (K_D of 4.03×10^{-4} M), model simulations show that protein to peptide ratios of 1:25 to 1:1000 provide protein release rates from 100% to 20% of total protein over 10 days. For the strong binding peptide system (K_D of 8.73×10^{-5} M), a similar range of release rates is achieved using protein to peptide ratios of only 1:10 to 1:100.

3.6. Effect of hydrogel geometry on protein release

To determine whether hydrogel geometry affects protein release, we used the model to compare protein release from a conical geometry (which mimics our experimental set-up, see Fig. 2B) to a cylindrical geometry, while keeping L constant. As shown in Fig. 7, protein release from the hydrogel is slower from the cylindrical (flat) geometry. This reflects the greater effective length for diffusion (i.e., the volume of the gel/interfacial area with the release medium) for the cylindrical vs. conical geometry.

4. Discussion

The mathematical model presented is able to provide insight into how physical parameters affect protein release profiles from single species affinity-based systems. A set of general guiding principles were deduced from an asymptotic analysis of the governing equations and can be used as a predictive tool to select a set of parameters that achieve a desired protein release profile. Such principles have been missing in prior publications [17,19,21–23]. Our model and scaling analysis provide a coherent picture for controlling release in single species affinity-based systems.

An asymptotic analysis, detailed in the supplementary information (Section S3), reveals that protein release from affinity-based systems falls into one of three regimes summarized in Table 1 and represented graphically in Fig. 8. In the first regime, the unbinding dynamics of the complex are fast ($\beta \gg 1$), i.e., diffusion is the rate-determining step, and a small proportion of peptides have been converted to complex ($\gamma \ll 1$) at the beginning of the experiment. This regime produces release over a single timescale, $\frac{L^2\left(1+\frac{C_{pep,T}}{K_D}\right)}{D}$. This demonstrates that the release time depends only on K_D and not the individual values of k_{off} and k_{on}. It is also independent of the amount of protein in the gel, which we (Fig. S1) and others [36] have observed experimentally. Furthermore, if $\frac{C_{pep,T}}{K_D} \ll 1$, the release time is independent of $C_{pep,T}$ and K_D as well. Thus, in regime 1, the concentration of binding ligand must be greater than K_D to achieve affinity-based release. If the concentration of binding ligand is lower than K_D, the equilibrium is shifted towards free peptide and protein, which will result in unaltered diffusional protein release from the gel.

Regime 2 represents another case of diffusion-controlled dynamics ($\beta \gg 1$), but where there is a large proportion of complexed peptides relative to uncomplexed ones ($\gamma \gg 1$). In this case, a two-stage release profile is obtained: initial release occurs over a timescale of $\frac{L^2}{D}\left(1+\frac{1}{\alpha}\right)$ until the protein concentration drops to $\frac{k_{off}}{k_{on}}$, after which the remainder of the protein is released over a timescale of $\frac{L^2(1+\gamma/\alpha)}{D}$. The timescale for the fast, initial release can be written as $\frac{L^2\left(1+\frac{C_{pep,T}}{C_{pro,0}}\right)}{D}$; it depends on the total peptide and initial equilibrium free protein concentration, and through the latter on K_D which determines the equilibrium. The comments from regime 1 for the longer timescale of $\frac{L^2(1+\gamma/\alpha)}{D}$ also apply here.

In regime 3 where $\beta \ll 1$, the decomplexation of bound protein is slow relative to diffusion $\left(\frac{1}{k_{off}} \gg \frac{L^2}{D}\right)$. Any free protein produced by decomplexation of the protein–peptide pair is also negligible relative to existing free protein concentration within the gel. This restriction can provide a more accurate lower bound on β for this regime: $\beta \ll min\left[1, \frac{(\gamma+1)}{\gamma\alpha}\right]$ (see SI, Section S3). In this regime nearly all the free protein is initially released from the gel over the diffusion timescale, $\frac{L^2}{D}$. The initial fast diffusive release is followed by the slower decomplexation and release of the bound protein over the timescale of $\frac{1}{k_{off}}$.

Let us consider the transition between the first/second regime and the third regime, which typically occurs when $\beta = \frac{L^2 k_{off}}{D} \approx 1$. Given that protein diffusivity through our gel does not change, either k_{off} or L

Table 1
Regimes of protein release from affinity-based systems.

Regime	Dominant dynamics	Restrictions on α and γ	Timescale of release
1	Diffusion controlled $\beta>>1\left(\frac{L^2}{D} \gg \frac{1}{k_{off}}\right)$ [more strictly $\beta \gg \min(1, \alpha(\gamma+1)/\gamma)$]	Peptides mostly uncomplexed $\gamma << 1$	Bound and free protein are released together over a single timescale $\frac{L^2(1+\gamma/\alpha)}{D} = \frac{L^2\left(1+\frac{C_{pep,T}}{K_D}\right)}{D}$
2	Diffusion controlled $\beta>>1\left(\frac{L^2}{D} \gg \frac{1}{k_{off}}\right)$ [more strictly $\beta \gg \min(1, \alpha(\gamma+1)/\gamma)$]	Peptides mostly complexed $\gamma >> 1$	Initially the timescale is $\frac{L^2}{D}\left(1+\frac{1}{\alpha}\right) = \frac{L^2}{D}\left(1+\frac{C_{pep,T}}{C_{pro,0}}\right)$ until protein concentration drops to $\frac{k_{off}}{k_{on}}$ after which it is $\frac{L^2(1+\gamma/\alpha)}{D} = \frac{L^2\left(1+\frac{C_{pep,T}}{K_D}\right)}{D}$
3	Unbinding (kinetically) controlled $\beta<<1\left(\frac{1}{k_{off}} \gg \frac{L^2}{D}\right)$	$\alpha \gg \frac{\beta\gamma}{(\gamma+1)}$	Initially all free protein is released over the timescale $\frac{L^2}{D}$ followed by slower release over the timescale $\frac{1}{k_{off}}$.

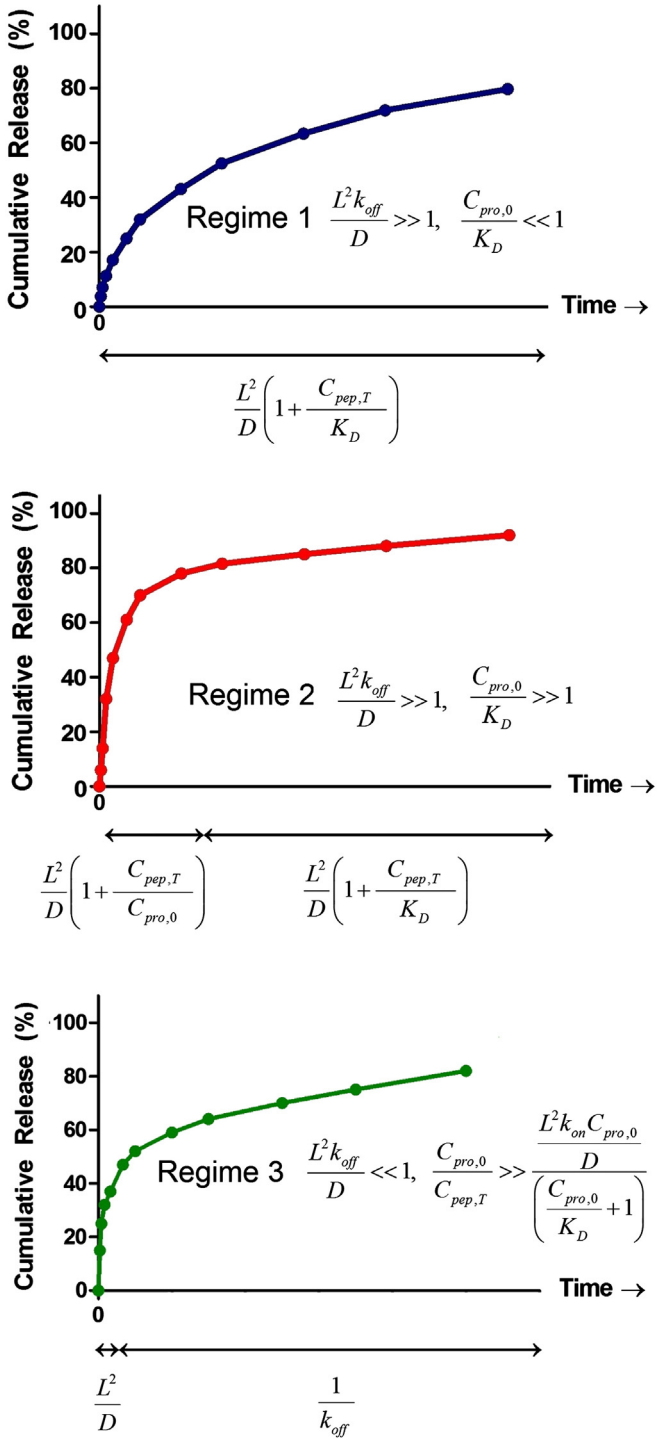

Fig. 8. Three regimes of release describe affinity-based release of therapeutic protein from a polymeric matrix immobilized with an affinity-binding ligand (peptide). The timescale for each phase of release is shown on the *x*-axis. L is the thickness of the delivery matrix (usually a hydrogel), D is the diffusivity of the protein through the delivery matrix, $C_{pep,T}$ is the total concentration of the peptide bound to the delivery matrix, C_{pro} is the equilibrium protein concentration, $C_{pro,0}$ is the initial protein concentration, K_D is the dissociation constant of the affinity pair, and k_{on} *and* k_{off} are the association and dissociation rates for the affinity complex respectively.

needs to be modified for our affinity-based system to observe changes in release. It is more feasible to modify the thickness of the hydrogel than the binding kinetics. If gel thickness is kept constant at 4 mm, as in our experiments, a k_{off} of $<10^{-7}$ s^{-1} is required for $\beta \approx 1$. This translates to a complex with a lifetime of ~3 months, stronger than the strongest known protein–protein complexes of colicin-immunity proteins which have a lifetime of 2 weeks [34,35]. However, if gel thickness is sufficiently decreased, it is possible to achieve $\beta \ll 1$ for physically relevant k_{off} values. More precisely, in order to observe a transition to the unbinding-controlled regime (regime 3, $\left(\frac{1}{k_{off}} \gg \frac{L^2}{D}\right)$), the thickness, L, would need to be below the order of $\sqrt{\frac{D}{k_{off}}}$. This was observed by Lin and Metters [19] who used very thin gels ($L = 0.28$ mm). As they varied k_{off} from 10^{-2} s^{-1} to 10^{-5} s^{-1}, they noticed a change in protein release from their gels. This occurred because β transitions from greater than 1 (78.4) to less than 1 (0.0784) over this range of k_{off} values, thereby changing the protein release rate from diffusion-controlled to unbinding-controlled. This shift is not observed in our affinity-based system because β is always much greater than unity for a gel thickness of 4 mm when considering physically relevant binding kinetics (see SI, Table S2). Notably, our overall duration of sustained release was much longer (10 days) than that of Lin and Metters (8 h).

The information provided by the above analysis can be used to design gels with desired release profiles. In regime 1, the rate of protein release decreases smoothly over a single timescale. In regimes 2 and 3, there are two distinct timescales: an initially fast release rate, followed by a more gradual one. The two timescales in regime 2 are related as they are both proportional to L^2/D whereas the two timescales in regime 3 can be independently controlled by separately tuning L^2/D and k_{off}, as long as $\alpha \gg \frac{\beta\gamma}{(\gamma+1)}$ and $L << \sqrt{\frac{D}{k_{off}}}$. Another key difference between regimes 2 and 3 is that all of the complexed protein remains in the bound state throughout the fast mode for regime 3 while approximately half of the complexed protein undergoes unbinding in the initial fast stage for regime 2. Thus, the affinity-based system allows the tuning, not only of the timescales of release, but also of the amounts of protein delivered in each stage. The dual timescale release can be useful for an application in which an initial bolus delivery of protein is desired, followed by a longer sustained release. Lastly, while release in the first two regimes is dependent on the shape of the gel, in the second stage of regime 3, it is not. This is because the slow stage in regime 3 is governed solely by the kinetics of the unbinding reaction (k_{off}).

Since our experimental system was always in regime 1, it was feasible to further analyze how individual parameters (K_D and k_{off}, protein to peptide ratio, geometry) affect the timescale of protein release for our system. Varying k_{on} and k_{off} within a physically relevant range did not affect the release rate because physically relevant rates of association and dissociation are fast relative to the timescale of protein diffusion through the gel ($\beta \gg 1$, Fig. 4). It is well known that modulating the binding strength of the affinity interaction (K_D) results in different rates of protein release [8,19,23] and we observed a similar trend using our model (Fig. 5). For example, using a protein to peptide concentration ratio of 1:100, tunable protein release from <10% to >90%, total release in 10 days is possible. As the strength of the binding interaction increases, the peptide excess required to achieve varying protein release profiles decreases.

We, and others, have experimentally observed that changing the protein to binding ligand ratio can modify protein release profiles [8,16,17,19] and this was verified by our model (Fig. 6). Importantly, from the asymptotic analysis, it has become clear that this can only be achieved by tuning the concentration of the binding ligand as the timescale of release is independent of protein concentration $\left[\frac{L^2\left(1+\frac{C_{pep,T}}{K_D}\right)}{D}\right]$ (SI, Fig. S1) [36].

The final piece of validation for the mathematical model is the comparison of the simulation results with our experimental data for two separate SH3 fusion proteins (SH3-rhFGF2 and SH3-ChABC) that were released from a peptide-modified hydrogel (Fig. 3) in normalized co-ordinates. Dimensionless analysis of our experimental system ($L = 4$ mm and $D = 1.07 \times 10^{-4}$ mm^2 s^{-1} for SH3-rhFGF2 or 8.25×10^{-5} mm^2 s^{-1} for SH3-ChABC) revealed that protein

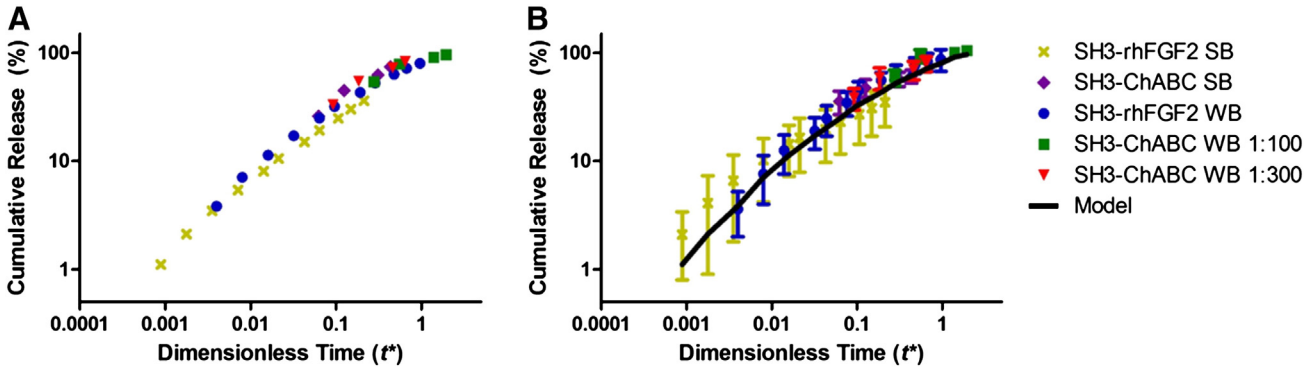

Fig. 9. A) Model simulations and B) experimental data shown with a representative model simulation (solid black line) collapse to form a master curve when plotted against an appropriately normalized time variable.

release will always fall within regime 1. Remarkably, all of our model simulations (Fig. 9A) and experimental data (Fig. 9B) can be collapsed onto a single master curve when the release time is expressed as a fraction of the characteristic timescale of release for each system, i.e., $t^* = t/\left[\frac{L^2}{D}\left(1+\frac{C_{pep,T}}{K_D}\right)\right]$. The small discrepancy in the master curve for the simulations (Fig. 9A) is a weak bias introduced by the inclusion of the dynamics of the release medium in the simulations, a factor that was not accounted for in the scaling analysis (see S3). Thus, irrespective of the individual parameters in the experimental system, as long as the system is in regime 1 (see Table 1), the cumulative release is a function of a single variable — the normalized time, t^*. This is a powerful result that can aid the design of an affinity-based release system with a preselected release period. For example, let us say that a cumulative release of 70% is required from the gel over a time of 3 days. From the master curve, for 70% release, a dimensionless time of $t^* \approx 0.45$ must elapse. From the definition of t^*, one can deduce that L, D $C_{pep,T}$ and K_D should be chosen to ensure that the quantity $\frac{L^2}{D}\left(1+\frac{C_{pep,T}}{K_D}\right)$ is about 6.7, and that the restrictions accompanying regime 1 are satisfied. Note that the master curve depends on the geometry of release (in our case, the tube with a conical bottom). But for any new geometry, a *single* experiment or simulation is sufficient to establish the master curve, again, as long as the release is designed to be in regime 1. Then no further experiments or simulations are required.

We also showed, for the first time, that the gel geometry can greatly affect the protein release profile (Fig. 7), particularly for regimes 1 and 2. This information is key when altering the geometry of the hydrogel to more clinically relevant geometries, such as flat (thin slab) geometry, which is expected for injection into the intrathecal space for local delivery to the injured spinal cord [37].

The mathematical model also provided us with insight into our experimental data. For example, we had to apply a correction factor to our experimental protein release profiles (SI, Figs. S5 and S6) to account for protein loss during freeze/thaw processing of samples before enzyme-linked immunosorbent assay (ELISA) or bicinchoninic acid (BCA) assay quantification. While it is common practice to freeze protein samples at −20 °C or −80 °C [38–40] to preserve activity during long-term storage, protein denaturation from aggregation at the ice/water interface during freeze/thaw processing before ELISA quantification is unavoidable [31,32]. This highlights the need to perform stability studies on any experimental protein in order to fully understand its *in vitro* release.

5. Conclusions

A mathematical model was developed to improve our understanding of the mechanisms that control protein release from affinity-based drug delivery systems. Using a comprehensive asymptotic analysis, we describe three regimes of protein release, wherein one or two stages of release are possible. We highlight that, initially, it is necessary to analyze the effects of the system as a whole because the individual factors are highly interdependent. In the case of our SH3/SH3-binding peptide affinity system, which always falls within regime 1, we found that the rate of dissociation (k_{off}) did not impact protein release profiles when K_D is kept constant; however, the strength of the affinity interaction (K_D), the concentration of peptide present in the system, and the hydrogel geometry could all be varied to tune protein release. The model was validated by comparison to experimental data for two proteins. This agreement was further strengthened when all data collapsed to a single master curve when plotted against an appropriately normalized time variable. Ultimately, the model developed herein and its scaling analysis is a useful tool for understanding the mechanisms of affinity-controlled release and predicting release profiles.

Supplementary data to this article can be found online at http://dx.doi.org/10.1016/j.jconrel.2014.10.032.

Acknowledgments

We are grateful to the Natural Sciences and Engineering Research Council of Canada (NSERC; Discovery grant to MSS; Vanier scholarship to MP) and the Ontario Graduate Scholarship (OGS; to KV) for funding this research.

References

[1] T. Patel, J. Zhou, J.M. Piepmeier, W.M. Saltzman, Polymeric nanoparticles for drug delivery to the central nervous system, Adv. Drug Deliv. Rev. 64 (2012) 701–705.
[2] D.A. LaVan, T. McGuire, R. Langer, Small-scale systems for *in vivo* drug delivery, Nat. Biotechnol. 21 (2003) 1184–1191.
[3] A.M. Alkilany, L.B. Thompson, S.P. Boulos, P.N. Sisco, C.J. Murphy, Gold nanorods: their potential for photothermal therapeutics and drug delivery, tempered by the complexity of their biological interactions, Adv. Drug Deliv. Rev. 64 (2012) 190–199.
[4] A.K. Salem, P.C. Searson, K.W. Leong, Multifunctional nanorods for gene delivery, Nat. Mater. 2 (2003) 668–671.
[5] K. Vulic, M.S. Shoichet, Tunable growth factor delivery from injectable hydrogels for tissue engineering, J. Am. Chem. Soc. 134 (2012) 882–885.
[6] N.X. Wang, H.A. von Recum, Affinity-based drug delivery, Macromol. Biosci. 11 (2011) 321–332.
[7] D.S. Pisal, M.P. Kosloski, S.V. Balu-Iyer, Delivery of therapeutic proteins, J. Pharm. Sci. 99 (2010) 2557–2575.
[8] D.J. Maxwell, B.C. Hicks, S. Parsons, S.E. Sakiyama-Elbert, Development of rationally designed affinity-based drug delivery systems, Acta Biomater. 1 (2005) 101–113.
[9] S.M. Willerth, P.J. Johnson, D.J. Maxwell, S.R. Parsons, M.E. Doukas, S.E. Sakiyama-Elbert, Rationally designed peptides for controlled release of nerve growth factor from fibrin matrices, J. Biomed. Mater. Res. 80 (2007) 13–23.
[10] G. Tae, M. Scatena, P.S. Stayton, A.S. Hoffman, PEG-cross-linked heparin is an affinity hydrogel for sustained release of vascular endothelial growth factor, J. Biomater. Sci. Polym. Ed. 17 (2006) 187–197.
[11] J.J. Yoon, H.J. Chung, H.J. Lee, T.G. Park, Heparin-immobilized biodegradable scaffolds for local and sustained release of angiogenic growth factor, J. Biomed. Mater. Res. 79A (2006) 934–942.
[12] T. Nie, A. Baldwin, N. Yamaguchi, K.L. Kiick, Production of heparin-functionalized hydrogels for the development of responsive and controlled growth factor delivery systems, J. Control. Release 122 (2007) 287–296.

[13] Y.-C. Ho, F.-L. Mi, H.-W. Sung, P.-L. Kuo, Heparin-functionalized chitosan-alginate scaffolds for controlled release of growth factor, Int. J. Pharm. 376 (2009) 69–75.
[14] J.M. Wu, Y.Y. Xu, Z.H. Li, X.Y. Yuan, P.F. Wang, X.Z. Zhang, Y.Q. Liu, J. Guan, Y. Guo, R.X. Li, H. Zhang, Heparin-functionalized collagen matrices with controlled release of basic fibroblast growth factor, J. Mater. Sci. Mater. Med. 22 (2010) 107–114.
[15] O. Jeon, C. Powell, L.D. Solorio, M.D. Krebs, E. Alsberg, Affinity-based growth factor delivery using biodegradable, photocrosslinked heparin-alginate hydrogels, J. Control. Release 154 (2011) 258–266.
[16] M.M. Pakulska, K. Vulic, M.S. Shoichet, Affinity-based release of chondroitinase ABC from a modified methylcellulose hydrogel, J. Control. Release 171 (2013) 11–16.
[17] M.D. Wood, S.E. Sakiyama-Elbert, Release rate controls biological activity of nerve growth factor released from fibrin matrices containing affinity-based delivery systems, J. Biomed. Mater. Res. 84 (2008) 300–312.
[18] S.E. Sakiyama-Elbert, J.A. Hubbell, Development of fibrin derivatives for controlled release of heparin-binding growth factors, J. Control. Release 65 (2000) 389–402.
[19] C.C. Lin, A.T. Metters, Metal-chelating affinity hydrogels for sustained protein release, J. Biomed. Mater. Res. 83 (2007) 954–964.
[20] C.C. Lin, A.T. Metters, Enhanced protein delivery from photopolymerized hydrogels using a pseudospecific metal chelating ligand, Pharm. Res. 23 (2006) 614–622.
[21] A.S. Fu, T.R. Thatiparti, G.M. Saidel, H.A. von Recum, Experimental studies and modeling of drug release from a tunable affinity-based drug delivery platform, Ann. Biomed. Eng. 39 (2011) 2466–2475.
[22] K.C. Koehler, K.S. Anseth, C.N. Bowman, Diels–Alder mediated controlled release from a poly(ethylene glycol) based hydrogel, Biomacromolecules 14 (2013) 538–547.
[23] T.-H. Fan, B. Soontornworajit, M. Karzar-Jeddi, X. Zhang, Y. Wang, An aptamer-functionalized hydrogel for controlled protein release: a modeling study, Soft Matter 7 (2011) 9326–9334.
[24] M.D. Wood, G.H. Borschel, S.E. Sakiyama-Elbert, Controlled release of glial-derived neurotrophic factor from fibrin matrices containing an affinity-based delivery system, J. Biomed. Mater. Res. 89A (2009) 909–918.
[25] I. Freeman, S. Cohen, The influence of the sequential delivery of angiogenic factors from affinity-binding alginate scaffolds on vascularization, Biomaterials 30 (2009) 2122–2131.
[26] J. Crank, The Mathematics of Diffusion, Oxford Clarendon Press, 1956.
[27] C. Geankoplis, Transport Processes and Separation Process Principles (Includes Unit Operations) Fourth Edition, Prentice Hall Press, 2003.
[28] J.M. Nitsche, G. Balgi, Hindered Brownian diffusion of spherical solutes within circular cylindrical pores, Ind. Eng. Chem. Res. 33 (1994) 2242–2247.
[29] R.J. Phillips, W.M. Deen, J.F. Brady, Hindered transport of spherical macromolecules in fibrous membranes and gels, AIChE J 35 (1989) 1761–1769.
[30] J.-P. Demers, A. Mittermaier, Binding mechanism of an SH3 domain studied by NMR and ITC, J. Am. Chem. Soc. 131 (2009) 4355–4367.
[31] E. Cao, Y. Chen, Z. Cui, P.R. Foster, Effect of freezing and thawing rates on denaturation of proteins in aqueous solutions, Biotechnol. Bioeng. 82 (2003) 684–690.
[32] M.C. Manning, D.K. Chou, B.M. Murphy, R.W. Payne, D.S. Katayama, Stability of protein pharmaceuticals: an update, Pharm. Res. 27 (2010) 544–575.
[33] S.M. Larson, A.R. Davidson, The identification of conserved interactions within the SH3 domain by alignment of sequences and structures, Protein Sci. 9 (2000) 2170–2180.
[34] M. Črnigoj, Z. Podlesek, M. Budič, D. Žgur-Bertok, The *Escherichia coli* uropathogenic-specific-protein-associated immunity protein 3 (Imu3) has nucleic acid -binding activity, BMC Microbiol. 14 (2014) 1–8.
[35] W. Li, A.H. Keeble, C. Giffard, R. James, G.R. Moore, C. Kleanthous, Highly discriminating protein–protein interaction specificities in the context of a conserved binding energy hotspot, J. Mol. Biol. 337 (2004) 743–759.
[36] Y.-I. Chung, G. Tae, S. Hong Yuk, A facile method to prepare heparin-functionalized nanoparticles for controlled release of growth factors, Biomaterials 27 (2006) 2621–2626.
[37] M.C. Jimenez Hamann, E.C. Tsai, C.H. Tator, M.S. Shoichet, Novel intrathecal delivery system for treatment of spinal cord injury, Exp. Neurol. 182 (2003) 300–309.
[38] R.A. Peattie, D.B. Pike, B. Yu, S. Cai, X.Z. Shu, G.D. Prestwich, M.A. Firpo, R.J. Fisher, Effect of gelatin on heparin regulation of cytokine release from hyaluronan-based hydrogels, Drug Deliv. 15 (2008) 389–397.
[39] S.J. Taylor, J.W. McDonald III, S.E. Sakiyama-Elbert, Controlled release of neurotrophin-3 from fibrin gels for spinal cord injury, J. Control. Release 98 (2004) 281–294.
[40] S.E. Sakiyama-Elbert, J.A. Hubbell, Controlled release of nerve growth factor from a heparin-containing fibrin-based cell ingrowth matrix, J. Control. Release 69 (2000) 149–158.